Published in final edited form as:
Nat Cell Biol. 2004 April ; 6(4): 343–350. doi:10.1038/ncb1115.

Gating of CFTR by the STAS domain of SLC26 transporters

Shigeru B. H. Ko[1,3], **Weizhong Zeng**[1], **Michael R. Dorwart**[1,2], **Xiang Luo**[1], **Kil Hwan Kim**[1], **Linda Millen**[1], **Hidemi Goto**[3], **Satoru Naruse**[3], **Abigail Soyombo**[1], **Philip J. Thomas**[1], and **Shmuel Muallem**[1,4]

[1]Department of Physiology, University of Texas Southwestern Medical Center at Dallas, Dallas, TX 75390-9040, USA.

[2]Graduate program in Molecular Biophysics, University of Texas Southwestern Medical Center at Dallas, Dallas, TX 75390-9040, USA.

[3]Division of Gastroenterology, Department of Medicine, Nagoya University Graduate School of Medicine, Nagoya 466-8550, Japan.

Abstract

Chloride absorption and bicarbonate secretion are vital functions of epithelia[1–6], as highlighted by cystic fibrosis and diseases associated with mutations in members of the SLC26 chloride-bicarbonate exchangers. Many SLC26 transporters (SLC26T) are expressed in the luminal membrane together with CFTR[7], which activates electrogenic chloride-bicarbonate exchange by SLC26T[8]. However, the ability of SLC26T to regulate CFTR and the molecular mechanism of their interaction are not known. We report here a reciprocal regulatory interaction between the SLC26T DRA, SLC26A6 and CFTR. DRA markedly activates CFTR by increasing its overall open probablity (NP_o) sixfold. Activation of CFTR by DRA was facilitated by their PDZ ligands and binding of the SLC26T STAS domain to the CFTR R domain. Binding of the STAS and R domains is regulated by PKA-mediated phosphorylation of the R domain. Notably, CFTR and SLC26T co-localize in the luminal membrane and recombinant STAS domain activates CFTR in native duct cells. These findings provide a new understanding of epithelial chloride and bicarbonate transport and may have important implications for both cystic fibrosis and diseases associated with SLC26T.

Chloride absorption and bicarbonate secretion are tightly associated processes vital to the function of all epithelia, including the respiratory, reproductive and gastro-intestinal systems. Their critical importance is reflected in cystic fibrosis, in which aberrant chloride absorption and bicarbonate secretion are central to epithelial tissue destruction[1,2]. Chloride absorption and bicarbonate secretion occur in the ductal systems of secretory glands, or their equivalents[3,4], and surface epithelial cells in the gastro-intestinal tract[5]. In spite of the physiological and pathological importance of these processes, the mechanism and control of epithelial chloride absorption and bicarbonate secretion remains obscure.

Epithelial chloride absorption and bicarbonate secretion are tightly coupled. The discovery that the pancreatic juice of cystic fibrosis patients is low in bicarbonate and high in chloride[6] suggests that the function of CFTR is associated with bicarbonate secretion. Because CFTR

[4]Correspondence should be addressed to S.M. (shmuel.muallem@utsouthwestern.edu).

Note: Supplementary Information is available on the Nature Cell Biology website.

COMPETING FINANCIAL INTERESTS

The authors declare that they have no competing financial interests.

functions as a cAMP-regulated chloride channel[9] that can also conduct some bicarbonate[10], models to explain chloride absorption and bicarbonate secretion were constructed in which CFTR operates in parallel with a chloride-bicarbonate exchanger in the luminal membrane of epithelia[3]. However, several features of this simple model are not compatible with key properties of epithelial bicarbonate secretion[11].

With the discovery of the SLC26 family of chloride and bicarbonate transporters (SLC26T), a new view of epithelial chloride and bicarbonate transport emerged. This family consists of at least ten genes, each of which may have several splice variants. Mutations in some members are linked to human diseases[7,12–14] caused by defective anion transport[8]. Several members show tissue-restricted expression[14, 15], whereas others are widespread[7, 8]. Most members are expressed in the luminal membrane[7,16]. Characterization of anion transport by three family members — down-regulated in adenoma (DRA)[17], Pendrin[18] and SLC26A6 (refs 19) — demonstrated that all function as chloridebicarbonate exchangers. This suggests that SLC26Ts are responsible for a luminal chloride-bicarbonate exchange. Key recent findings demonstrated that the SLC26T are electrogenic[8,20] and are markedly activated by CFTR[8]. These properties can account for most forms of epithelial chloride absorption and bicarbonate secretion and explain the central role of CFTR in both processes. Tight control of epithelial chloride and bicarbonate transport requires that SLC26T and CFTR be reciprocally regulated. To address this question, we examined the molecular and functional interactions between CFTR and the SLC26T DRA and SLC26A6.

The carboxyl terminus of CFTR[21], DRA[22] and SLC26A6 (ref. 23) binds to EBP50. Fig. 1a shows that when CFTR and DRA were expressed at low levels, deletion of the PDZ ligand of CFTR prevented co-immunoprecipitation of CFTR with DRA. In contrast, when ΔC-CFTR (CFTR with a truncation of the C-terminal PDZ motif) and DRA were expressed at high levels, DRA could be co-immunoprecipitated with ΔC-CFTR, indicating that additional domains of CFTR and DRA mediate their association. Accordingly, the R domain (amino acids 590–858 of CFTR) could be co-immunoprecipitated with DRA (Fig. 1b).

A potential CFTR-interacting domain in DRA was suggested by the recent identification of a conserved domain in the C-terminal tail of all SLC26Ts, the STAS domain[24]. Co-expression of the STAS (amino acids 518–713 of mDRA) and R domains markedly increased the amount of the STAS domain (Fig. 1c; $n > 10$), consistent with their physical interaction that stabilizes the STAS domain. CFTR also increased amounts of the STAS domain (Fig. 1c). Significantly, deletion of the STAS domain from DRA prevented its binding to CFTR and the R domain (Fig. 1d). Finally, the STAS and R domains could be reciprocally co-immunoprecipitated (Fig. 1d).

Interestingly, phosphorylation of the R domain enhanced its binding to the STAS domain. Co-immunoprecipitation of the STAS and R domains was higher in extracts prepared from cells stimulated with forskolin, which activates PKA, than cells treated with H89, which inhibits PKA (Fig. 1e, 1.8 ± 0.1-fold). Furthermore, a recombinant glutathione *S*-transferase (GST)–R domain functioned poorly in pulling down the STAS domain from cell lysates (Fig. 1f). However, phosphorylation of the R domain markedly improved the pull-down ($n = 3$). Similarly, the phosphorylated R domain pulled down DRA, but not ΔSTAS-DRA, (data not shown). Together, these results indicate that CFTR and DRA interact through their R and STAS domains, respectively, and that the interaction is augmented by phosphorylation of the R domain.

We then determined the role of the PDZ ligands and the STAS domain in activation of DRA by CFTR (see Supplementary Information, Fig. S1). When expressed at low levels, deletion of the PDZ ligands of CFTR, DRA, or both, reduced activation of DRA-mediated chloride/

hydroxyl exchange by CFTR (see Supplementary Information, Fig. S1a, f, i). However, when ΔC-CFTR and ΔC-DRA were over-expressed, ΔC-CFTR still maximally activated ΔC-DRA (see Supplementary Information, Fig. S1h, i). Deletion of the R domain prevented activation of DRA by CFTR, even when the proteins were overexpressed (see Supplementary Information, Fig. S1j, k). This indicates that the R domain is required for activation of DRA by CFTR. Most notably, overexpression of the STAS domain inhibited activation of DRA by CFTR (see Supplementary Information, Fig. S1l, m). This inhibition is most probably caused by competition of the STAS domain with DRA for binding to the R domain (Fig. 1).

Activation of CFTR by SLC26T is shown in Fig. 2a, b. Although both are electrogenic[8], expression of *mDRA* (Fig. 2) or *SLC26A6* (data not shown) in HEK293 cells did not generate appreciable chloride current, probably because they catalyse low turnover. Expression of CFTR resulted in a chloride current of 49.8 ± 1.6 pA/pF. Remarkably, co-expression of mDRA and CFTR increased CFTR current to 126.3 ± 3.6 pA/pF. As previously reported[25], CFTR activated hDRA chloride/hydroxyl exchange by 3.9 ± 0.36 fold (n = 3). Expression of hDRA stimulated CFTR current (Fig. 2; 106.1 ± 4.6 pA/pF), indicating that the mDRA and hDRA interact similarly with CFTR. Furthermore, mSLC26A6 also activated CFTR (91.3 ± 2.7 pA/pF), although mSLC26A6 was less effective than DRA.

Single-channel analysis revealed that DRA increased CFTR open probablility (P_o) approximately 2.2-fold (Fig. 2e) and the number of active channels per patch by a factor of two, thereby increasing the NP_o from 0.71 ± 0.11 to 3.65 ± 0.52 (Fig. 2f). Further analysis revealed that DRA had no effect on burst duration (τ_0), but decreased inter-burst duration (τ_c) from 3.5 ± 0.7 ms to 1.8 ± 0.2 ms, n = 4–6 (Fig. 2g, h). Western blot and surface biotinylation (Fig. 2i) failed to show increased expression of CFTR at the plasma membrane, suggesting that the increased NP_o was probably caused by an increased probability of detecting active channels in a patch.

Next, we examined the effect of the STAS domain on CFTR. The DRA STAS domain activated CFTR approximately threefold (Fig. 3a, b). Similarly, infusing cells with recombinant SLC26A6 STAS domain (maltose-binding protein (MBP)–A6STAS) activated CFTR approximately 1.8-fold. If the STAS domain activates CFTR by binding to the R domain, the STAS domain should not activate ΔR-CFTR. Similarly to previous reports[26], ΔR-CFTR was spontaneously active, with a chloride current approximately 30% of wild-type CFTR that was minimally activated by PKA (Fig. 3c, d). However, The STAS domain had no effect on the ΔR-CFTR, either before or after stimulation of PKA.

Single-channel analysis showed that the STAS domain increased CFTR P_o by approximately 3.5-fold and NP_o by a factor of seven (Fig. 3e–i). Similarly to DRA, the STAS domain had no effect on τ_0, but decreased τ_c from 3.6 ± 0.7 to 2.0 ± 0.4 ms. Western blotting and surface biotinylation showed no effect of the STAS domain upon expression of CFTR at the plasma membrane (Fig. 3j), indicating that the STAS domain activated CFTR mainly by affecting its gating.

Several mutations in DRA cause congenital chloride diarrhea (CLD), one of which is insertion of an isoleucine between positions 675 and 676 in hDRA[12], in the predicted second α-helix of the STAS domain (see Supplemntary Information, Fig. S2). The equivalent mutation in mDRA (DRA668i) and its STAS domain (STAS668i) were tested for their effect on CFTR activity. The mutant STAS domain bound to the R domain (Fig. 1e, lane 4). However, DRA668i and STAS668i inhibited, rather than stimulated, CFTR by 55% and 42%, respectively (Fig. 3a, g, i) by reducing P_o and NP_o by 35–40%. A plausible mechanism

by which DRA668i and STAS668i inhibit CFTR is by preventing an interaction of CFTR with endogenous SLC26T.

Infusion of a recombinant MBP–DRA STAS domain activated CFTR by approximately 75% (Fig. 4a, e). The advantage of using the recombinant protein is that it can be used to test activation of native CFTR. The recombinant STAS domain activated CFTR in freshly isolated parotid duct cells, similarly to CFTR expressed in HEK 293 cells (Fig. 4c–e).

Previous work showed that DRA and CFTR can be co-immunoprecipitated from the pancreas of wild-type, but not ΔF/ΔF (monozygote for deletion of F508 of CFTR) mice[8]. Unfortunately, the same anti-DRA antibodies were not suitable for immunolocalization studies. However, an anti-SLC26A6 antibody gave a good response in several rat tissues. Fig. 4f–n shows co-localization of SLC26A6 and CFTR in the pancreatic and parotid ducts and the small intestinal epithelium. Interestingly, most SLC26A6 was found in intralobular ducts and was rarely observed in the larger more distal ducts that did express CFTR (Fig. 4h). This localization may suggest an isoform-specific role in bicarbonate secretion.

The results presented here provide a new mechanism for regulation of CFTR activity, epithelial chloride absorption and bicarbonate secretion, and have important implications for both cystic fibrosis and CLD. Thus, regulatory interactions between the R domain of CFTR and the STAS domain of the SLC26T that is facilitated by their PDZ ligands markedly activates both transporters to increase CFTR NP_o and DRA activity by 5–7-fold. Such a pronounced activation can be viewed as approximating an ‘on–off ’ form of regulation.

The reciprocal activation of the SLC26T and CFTR has profound physiological implications and particular relevance to cystic fibrosis and CLD. The mechanism of chloride absorption and bicarbonate secretion by most CFTR-expressing tissues is not well understood. This is most clearly demonstrated in the pancreas and salivary glands, where the means by which their ducts produce a fluid that contains as little as 20 mM chloride and as much as 140 mM bicarbonate[3] remains unknown. A large portion of bicarbonate secretion by the pancreatic duct was shown to be conductive, and therefore it was suggested that this was mediated by CFTR[27]. However, CFTR alone can generate the observed gradients only if it can conduct bicarbonate, if the intracellular chloride concentration is less than 4 mM, and if the membrane potential across the duct luminal membrane is greater than −60 mV. The best available evidence indicates that the trans-epithelial voltage of the stimulated duct is approximately −30 mV[3,4]. With a basolateral membrane potential of −50 mV[27], the potential across the luminal membrane is approximately −20 to −30 mV. With an intracellular pH of between 7.2 and 7.3, even if the ducts reduce chloride to 4 mM at a luminal chloride concentration of 20 mM, the maximum possible luminal bicarbonate concentration is 80 mM.

An alternative mechanism that can explain all the known features of chloride absorption and bicarbonate secretion by these tissues is implicit in the current findings. In this model, depicted in Fig. 5, the ducts express consecutively two SLC26Ts with the relative stoichiometries of SLC26A6 and DRA (two bicarbonate per one chloride, and two chloride per one bicarbonate, respectively[8]). The SLC26T and CFTR in the bicarbonate-transporting complex are stabilized by their PDZ ligands. When fluid secretion is stimulated by PKA-activating agonists, the R domain is phosphorylated and interacts with the STAS domain to cause mutual activation of CFTR and the SLC26T. The proximal portion of the duct (where SLC26A6 is expressed) absorbs most of the chloride, whereas the distal portion concentrates bicarbonate to 140 mM while absorbing the residual chloride. Such a model is supported by the finding that luminal, but not basolateral, chloride-bicarbonate exchange is impaired in pancreatic and sub-mandibular gland ducts of ΔF/ΔF mice[28], by co-immunoprecipitation of

CFTR and DRA from ducts of wild-type (but not ΔF/ΔF) mice[8], and by co-expression of SLC26A6 and CFTR (Fig. 4).

The model in Fig. 5 can generate a fluid containing 20 mM chloride and 140 mM bicarbonate. With an intracellular chloride concentration of 4–10 mM[29,30], an SLC26A6-like transporter can reduce luminal chloride to 60 mM while increasing bicarbonate to at least 50 mM. Subsequently, a DRA-like transporter with a two-chloride/one-bicarbonate stoichiometry can reduce luminal chloride to 20 mM while increasing bicarbonate to more than 220 mM. However, the limited availability of chloride is sufficient for additional secretion of only approximately 20 mM bicarbonate. CFTR can then regulate bicarbonate secretion by secreting chloride to increase its luminal supply. Furthermore, CFTR further regulates chloride absorption and bicarbonate secretion by activating the SLC26T and by hyperpolarizing the voltage across the luminal membrane to limit the gradients generated by DRA to 20 mM luminal chloride and 140 mM luminal bicarbonate. Mutations in CFTR that result in destruction of the protein inhibit chloride absorption and bicarbonate secretion because of the lack of both chloride conductance and activation of the SLC26T. The model can also explain how mutations in CFTR that retain substantial chloride channel activity can cause cystic fibrosis. Aberrant activation of the native chloride-bicarbonate exchangers by these mutants[31] suggests that they cannot effectively activate the SLC26T.

METHODS

Plasmid construction

Wild-type CFTR cDNA in pCMV vector was provided by J. Rommens (Hospital for Sick Children, Toronto). Deletion of the last six amino acids of CFTR (ΔC-CFTR), was achieved by insertion of a stop codon into wild-type CFTR plasmid through site-directed mutagenesis. Primer sequence information is available on request. All constructs were verified by sequencing. The ΔR-CFTR construct (deletion of amino acids 708–835) was a generous gift from M. J. Welsh (University of Iowa). The cDNA encoding ΔR-CFTR was excised from the original vector and transferred to pCMV6. To prepare the haemagglutinin (HA)-tagged R domain, a PCR fragment encoding amino acids 590–858 was cloned into the pCMV-HA vector (Clontech, Palo Alto, CA).

pCl-neo mDRA was a gift from J. Melvin (University of Rochester, NY). hDRA was amplified from a human cDNA colon library (Clontech) with primers that added *Not*I sites to the 5′ and 3′ ends. The primers used were: forward: 5′-CGCCGCGGCCGCATGATTGAACCCTTTGGGAATC-3′ and reverse: 5′-CGCCGCGGCCGCTTAGAATTTTGTTTCAACTGGC-3′. The PCR product was inserted into the multiple cloning site at the *Not*I position of pCMV3.1. The presence and orientation of the insert was verified by sequencing. pCMV-Myc-DRA was prepared as previously described[8]. To obtain the Myc-tagged STAS domain, a PCR fragment encoding amino acids 518–713 of DRA was cloned into a pCMV-Myc vector. Several mutants — DRA P752X (ΔC-DRA), DRA N518X (DRA-ΔSTAS), DRA-I668–669ins (DRA668i) and STAS-I668–669ins (STAS668i) — were prepared by introducing the appropriate mutation. Constructs were verified by sequencing. Expression of proteins was verified by immunoblotting. The SLC26A6 clone was prepared as previously described[8].

Expression in HEK293 cells

Plasmids were co-transfected with a GFP plasmid (Invitrogen, Carlsbad, CA) into HEK293 cells using Lipofectamine and Plus reagent (Invitrogen). Empty pcDNA3.1 or pCMV-HA vectors were used to normalize the amount of DNA used in each transfection. Cells were used 24–72 h after transfection.

Preparation of phosphorylated GST–R and MBP–STAS domains of DRA and SLC26A6

GST and GST–R (amino acids 670–835) were expressed in a pGEX vector that was transformed into *Escherichia coli*. After induction with isopropyl-1-thio-β-D-galactopyranoside (IPTG), cells were pelleted, resuspended in lysis buffer, sonicated and the supernatant collected by centrifugation at 40,000*g* for 30 min. Proteins were captured on glutathione beads, and the beads washed five times. To prepare phosphorylated R domain, GST–R-domain beads were washed in PKA buffer (50 mM Tris-HCl at pH 7.5, 10 mM $MgCl_2$ and 0.1 mg ml^{-1} bovine serum albumine) and incubated with a PKA catalytic subunit and 5 μM ATP at 30 °C for 1 h. The beads were then washed and used for pull-down assays. MBP, MBP–STAS domain of DRA (amino acids 503–764 of hDRA) and MBP–STAS domain of SLC26A6 (amino acids 508–718 of SLC26A6) were expressed in pMAL-c2x that was transformed into *E. coli*. After induction and extraction as above, proteins were purified on amylose resin (New England Biolabs, Beverly, MA), according to the manufacturer's instructions.

Immunoblotting, co-immunoprecipitation, pull-down and immunolocalization assays

For biotinylation experiments, cells were incubated with 0.5 mg ml^{-1} EZ-LINK Sulfo-NHS-LC-biotin for 30 min at room temperature, washed with PBS and lysed. Biotinylated CFTR was isolated with avidin beads and recovered by heating at 95 °C for 3 min. Extracts were prepared by disruption of cells in ice-cold lysis buffer (20 mM Tris, 150 mM NaCl, 2mM EDTA, 1% Triton X-100, 0.2 mM phenyl methylsulphonyl fluoride, 10 μM leupeptine, 10 μM pepstatin and 10 μM aprotinin), incubation for 15–30 min, and collection by centrifugation. For co-immunoprecipitation, extracts were incubated with anti-HA (MMS-101P; Covance, Princeton, NJ), anti-Myc (sc-40; Santa Cruz Biotechnology, Santa Cruz, CA), anti-CFTR (M3A7; Upstate, Lake Placid, NY), or anti-R domain (13-1; R&D Systems, Minneapolis, MN) antibodies. Polyclonal anti-DRA antibodies were raised in rabbits against the C-terminal peptide of DRA[8] and polyclonal anti-SLC26A6 antibodies were raised against an N-terminal peptide of SLC26A6 (MDLRRRDYHMERPLLNQEHL). Extracts were incubated with antibodies and Protein G beads for 2–12 h at 4 °C. Beads were collected, washed three times with lysis buffer and proteins were recovered by heating in SDS sample buffer.

For pull-down assays, 50 μl of GST or GST–R domain beads were incubated with 130 μl of HEK 293 cell lysates expressing either green fluorescent protein, DRA, DRA(ΔSTAS) or STAS domain for 12–16 h at 4 °C. The beads were then washed four times before the proteins were released by incubation in sample buffer. Samples were separated by SDS–PAGE.

Preliminary experiments showed that the best localization can be obtained in rat and that the anti-DRA antibodies were not suitable for immunolocalization. Sections were prepared from the pancreas and small intestine. Cells were prepared from the salivary glands. Samples were fixed and permeabilized in cold Methanol. The monoclonal anti-R domain and polyclonal anti-SLC26A6 antibodies were used to test co-localization of CFTR and SLC26A6, respectively, using a previously described procedure[8].

Measurement of intracellular pH

Intracellular pH (pH_i) was measured with BCECF, as previously described[15]. Cells were perfused with Hepes-buffered Solution A: 140 mM NaCl, 5 mM KCl, 1 mM $MgCl_2$, 1 mM $CaCl_2$, 10 mM glucose and 10 mM HEPES (pH 7.4 with NaOH). Chloride-free solution was prepared by replacing chloride with gluconate. BCECF fluorescence was recorded at excitation wavelengths of 490 and 440 nm at a resolution of 2 s^{-1}. Changes in pH_i were

analysed by determining the rate of ΔpH_i per min from the first derivative (slope) of the changes in pH_i, and calculated as percentage of control.

Preparation of parotid duct cells

Single parotid duct cells were prepared by minor modifications of a previously described procedure[30]. Mouse parotid glands were minced and treated with 0.025% trypsin for 7 min at 37 °C. After stopping the reaction with 1.5 mg ml^{-1} soybean trypsin inhibitor, the tissue was further digested for 20 min with 70 U ml^{-1} collagenase CLSPA (Worthington, Lakewood, NJ). Cells were washed, suspended in solution A containing 1.5 mg ml^{-1} soybean trypsin inhibitor and kept on ice until use.

Electrophysiology

Macroscopic chloride-current recordings were made as previously described[30]. To isolate the chloride current, the pipette and bath solutions contained chloride as the only permeable anion. For whole-cell recording, the pipette solution contained 150 mM *N*-methyl-D-glucamine-Cl, 1 mM $MgCl_2$, 1 mM EGTA, 0.5 mM ATP and 10 mM HEPES at pH 7.3. The bath solution contained 150 mM *N*-methyl-D-glucamine-Cl, 1 mM $MgCl_2$, 1 mM $CaCl_2$ and 10 mM Hepes-Tris at pH 7.4. For cell-attached single-channel recording, the pipette solution was identical to the bath solution used for the whole-cell recording (solution A). Pipette resistance was 3–7 MΩ and the access resistance was approximately 10 MΩ. Seals of >10GΩ were produced on the cell surface. The cells were used to record single-channel current or to obtain the whole-cell configuration by gentle suction and/or voltage pulses of 0.5 V for 0.3–1 ms. Currents were recorded using the Axopatch 200B patch-clamp amplifier (Axon Instruments, Union City, CA). In all protocols, data were collected at 5 kHz and filtered at 1 kHz. During whole-cell recording, the membrane potential was held at −60 mV. For cell-attached single-channel recording, the pipette potential was held at +60 mV.

Channel open probability (P_o) was estimated using the equation:

where t_i is the time spent above a threshold set at 0.5 times channel current amplitude, T is the duration of the recording and N is the number of channels in a patch[32]. The number of active channels in a patch was determined from the number of simultaneously open channels during at least 15 min of recording. Because P_o of CFTR is 0.2–0.4, simultaneous opening of all active channels during the recording period are likely to be observed. The pclamp7 pSTAT program was used to determine P_o of multiple CFTR channels in a patch, making the assumption that the channels are identical and independent. As all recordings from cells expressing DRA or the STAS domain have multiple channel openings, mean open and close time could not be reliably determined. Alternatively, we determined burst (τ_0) and interburst (τ_c) durations according to the procedure and equations[32] that were used before to estimate mean burst and inter-burst intervals of CFTR in multi-channel patches[33].

$\tau_0 = (NP_o)T/(\text{number of openings})$ and $\tau_c = (N - NP_o)T/(\text{number of openings} - 1)$.

$$P_{\emptyset} = \sum_{i=l}^{N} t_i / TN$$

Statistical analysis

Results in all experiments are given as the mean ± s.e.m. of the indicated number of experiments. The results were analysed using paired or non-paired Student's *t*-test and ANOVA as appropriate.

Supplementary Material

Refer to Web version on PubMed Central for supplementary material.

Acknowledgments

This work was supported by grants DE12309, DK38938, cystic fibrosis Foundation grant MUALLE01G0 (to S.M.), DK49835 (to P.T.), traning grant GM-08203 (M.R.D.), Pancreas Research Foundation of Japan (to S.K.) and the Ministry of Education, Science, Technology, Sports and Culture, Japan, and the Uehara Memorial Foundation (to S.N.). S.B.H.K. was supported by the Japan Health Sciences Foundation.

References

1. Sokol RZ. Infertility in men with cystic fibrosis. Curr. Opin. Pulm. Med. 2001; 7:421–426. [PubMed: 11706320]
2. Wilschanski M, Durie PR. Pathology of pancreatic and intestinal disorders in cystic fibrosis. J. R. Soc. Med. 1998; 91(Suppl 34):40–49. [PubMed: 9709387]
3. Argent, BE.; Case, RM. Physiology of the Gastrointestinal Tract. 3rd ed.. Johnson, LR., editor. New York: Raven Press; 1994. p. 1473-1497.
4. Cook, DI.; Van Lennep, EW.; Roberts, ML.; Young, JA. Textbook of Physiology of the Gastrointestinal Tract. 3rd ed.. Johnson, LR., editor. New York: Raven Press; 1994. p. 1061-1117.
5. Kunzelmann K, Mall M. Electrolyte transport in the mammalian colon: mechanisms and implications for disease. Physiol Rev. 2002; 82:245–289. [PubMed: 11773614]
6. Hadorn B, Johansen PG, Anderson CM. Pancreozymin secretin test of exocrine pancreatic function in cystic fibrosis and the significance of the result for the pathogenesis of the disease. Can. Med. J. 1968; 98:377–384.
7. Mount DB, Romero MF. The SLC26 gene family of multifunctional anion exchangers. Pflugers Arch. 2004; 447:710–721. [PubMed: 12759755]
8. Ko SB, et al. A molecular mechanism for aberrant CFTR-dependent HCO_3^- transport in cystic fibrosis. EMBO J. 2002; 21:5662–5672. [PubMed: 12411484]
9. Sheppard DN, Welsh MJ. Structure and function of the CFTR chloride channel. Physiol Rev. 1999; 79:S23–S45. [PubMed: 9922375]
10. Poulsen JH, Fischer H, Illek B, Machen TE. Bicarbonate conductance and pH regulatory capability of cystic fibrosis transmembrane conductance regulator. Proc. Natl Acad. Sci. USA. 1994; 91:5340–5344. [PubMed: 7515498]
11. Sohma Y, Gray MA, Imai Y, Argent BE. HCO_3^- transport in a mathematical model of the pancreatic ductal epithelium. J. Membr. Biol. 2000; 176:77–100. [PubMed: 10882430]
12. Makela S, Kere J, Holmberg C, Hoglund P. SLC26A3 mutations in congenital chloride diarrhea. Hum. Mutat. 2002; 20:425–438. [PubMed: 12442266]
13. Superti-Furga A, et al. Achondrogenesis type IB is caused by mutations in the diastrophic dysplasia sulphate transporter gene. Nature Genet. 1996; 12:100–102. [PubMed: 8528239]
14. Everett LA, et al. Pendred syndrome is caused by mutations in a putative sulphate transporter gene (PDS). Nature Genet. 1997; 17:411–422. [PubMed: 9398842]
15. Lohi H, et al. Functional characterization of three novel tissue-specific anion exchangers SLC26A7, -A8, and -A9. J. Biol. Chem. 2002; 277:14246–14254. [PubMed: 11834742]
16. Haila S, et al. The congenital chloride diarrhea gene is expressed in seminal vesicle, sweat gland, inflammatory colon epithelium, and in some dysplastic colon cells. Histochem. Cell. Biol. 2000; 113:279–286. [PubMed: 10857479]
17. Melvin JE, Park K, Richardson L, Schultheis PJ, Shull GE. Mouse down-regulated in adenoma (DRA) is an intestinal Cl^-/HCO_3^- exchanger and is up-regulated in colon of mice lacking the NHE3 Na^+/H^+ exchanger. J. Biol. Chem. 1999; 274:22855–22861. [PubMed: 10428871]
18. Soleimani M, et al. Pendrin: an apical $Cl^-/OH^-/HCO_3^-$ exchanger in the kidney cortex. Am. J. Physiol. 2001; 280:F356–F364.

19. Wang Z, Petrovic S, Mann E, Soleimani M. Identification of an apical Cl^-/HCO_3^- exchanger in the small intestine. Am. J. Physiol. 2002; 282:G573–G579.
20. Xie Q, Welch R, Mercado A, Romero MF, Mount DB. Molecular characterization of the murine Slc26a6 anion exchanger: functional comparison with Slc26a1. Am. J. Physiol. 2002; 283:F826–F838.
21. Wang S, Yue H, Derin RB, Guggino WB, Li M. Accessory protein facilitated CFTR–CFTR interaction, a molecular mechanism to potentiate the chloride channel activity. Cell. 2000; 103:169–179. [PubMed: 11051556]
22. Lamprecht G, et al. The down regulated in adenoma (dra) gene product binds to the second PDZ domain of the NHE3 kinase A regulatory protein (E3KARP), potentially linking intestinal Cl^-/HCO_3^- exchange to Na^+/H^+ exchange. Biochemistry. 2002; 41:12336–12342. [PubMed: 12369822]
23. Lohi H, et al. Isoforms of the anion exchanger SLC26A6 mediate chloride and sulfate transport and have functional PDZ interaction domains. Am. J. Physiol. 2002; 284:C769–C779.
24. Aravind L, Koonin EV. The STAS domain — a link between anion transporters and antisigma-factor antagonists. Curr. Biol. 2000; 10:R53–R55. [PubMed: 10662676]
25. Chernova MN, et al. Acute regulation of the SLC26A3 congenital chloride diarrhoea anion exchanger (DRA) expressed in *Xenopus* oocytes. J. Physiol. 2003; 549:3–19. [PubMed: 12651923]
26. Ostedgaard LS, Baldursson O, Welsh MJ. Regulation of the cystic fibrosis transmembrane conductance regulator Cl^- channel by its R domain. J. Biol. Chem. 2001; 276:7689–7692. [PubMed: 11244086]
27. Ishiguro H, et al. Membrane potential and bicarbonate secretion in isolated interlobular ducts from guinea-pig pancreas. J. Gen. Physiol. 2002; 120:617–628. [PubMed: 12407075]
28. Lee MG, et al. Cystic fibrosis transmembrane conductance regulator regulates luminal Cl^-/HCO_3^- exchange in mouse submandibular and pancreatic ducts. J. Biol. Chem. 1999; 274:14670–14677. [PubMed: 10329661]
29. Ishiguro H, et al. Chloride transport in microperfused interlobular ducts isolated from guinea-pig pancreas. J. Physiol. 2002; 539:175–189. [PubMed: 11850511]
30. Zeng W, et al. Immuno and functional characterization of CFTR in submandibular and pancreatic acinar and duct cells. Am. J. Physiol. 1997; 273:C442–C455. [PubMed: 9277342]
31. Choi JY, et al. Aberrant CFTR-dependent HCO_3^- transport in mutations associated with cystic fibrosis. Nature. 2001; 410:94–97. [PubMed: 11242048]
32. Colquhoun, D.; Hawkes, AG. Single-channel Recording. Sakmann, B.; Neher, E., editors. New York: Plenum Press; 1983. p. 135-174.
33. Hanrahan JW, et al. Patch-clamp studies of cystic fibrosis transmembrane conductance regulator chloride channel. Methods Enzymol. 1998; 293:169–194. [PubMed: 9711609]

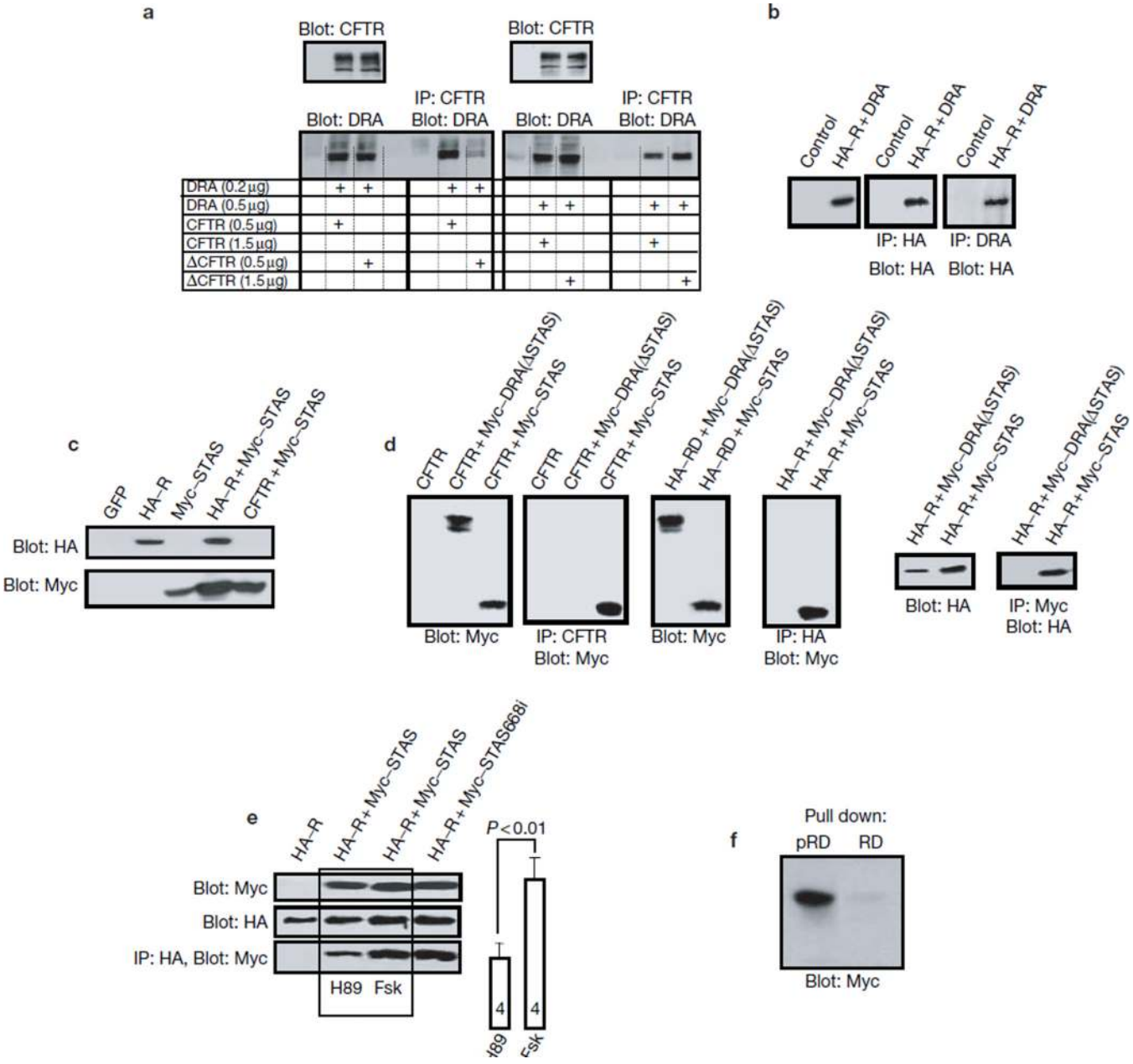

Figure 1.

Role of the PDZ ligands in the interaction between the STAS and R domains. (**a**) Extracts were prepared from HEK293 cells transfected with the indicated amount of cDNA encoding CFTR, ΔC-CFTR and mDRA, and used to test for co-immunoprecipitation of mDRA and CFTR. In the experiments with low protein expression (left), approximately 40 μg protein was used for blotting and approximately 400 μg protein for the co-immunoprecipitation. In the experiments with high protein expression (right), approximately 15 μg and 150 μg protein was used for blotting and co-immunoprecipitation, respectively. Blots are representative of three similar experiments. (**b**) Control cells (lane 1) and cells transfected with HA–R and wild-type mDRA were used to immunoprecipitate the R domain (second blot) or mDRA (third blot) and blot for the R domain (all blots). (**c–e**) Cells were transfected as indicated. In **c**, extracts were probed for protein expression. Panel **d** shows that CFTR

(left) and the R domain (right) co-immunoprecipitate the STAS domain, but not mDRA(ΔSTAS). The blots at the left show that the STAS domain co-immunoprecipitates the R domain. In **e**, cells transfected with the indicated constructs were treated for 15 min with 10 μM H89 or 5 μM forskolin, as indicated, before extraction. The bands from four experiments were scanned and the measured band densities are summarized as the mean ± s.e.m. (**f**) PKA-phosphorylated (pRD) and non-phosphorylated (RD) recombinant GST–R domains were used to pull down the STAS domain from cell extracts.

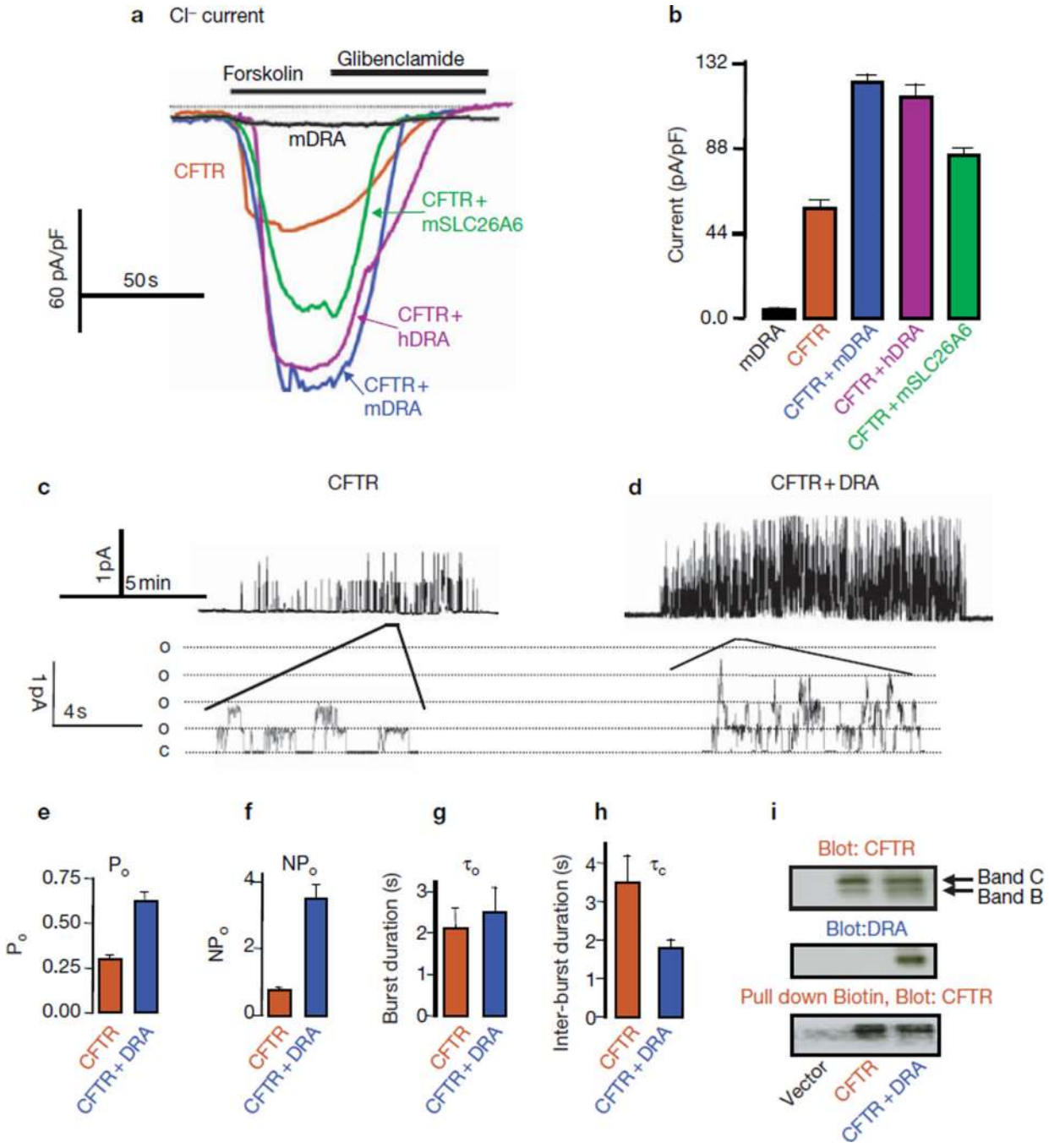

Figure 2.

Activation of CFTR by DRA and SLC26A6. (**a**) All traces and averages are colour-coded, as indicated. HEK293 cells transfected with mDRA (black), CFTR (brown), CFTR and mDRA (blue), CFTR and hDRA (purple), or CFTR and mSLC26A6 (green), were used to measure the whole-cell chloride current. Where indicated, cells were stimulated with 5 μM forskolin and inhibited with 100 μM glibenclamide. (**b**) A summary of four experiments under each condition in **a**. (**c, d**) Cells transfected with CFTR (**c**), or CFTR and mDRA (**d**), were used to record single-channel activity in cell-attached patches. Traces are from cells stimulated with forskolin for at least 5 min. (**e, f**) Averaged P_o (**e**) and NP_o (**f**) from four

experiments. (**g, h**) Averaged τ_0 and τ_c from six (CFTR) and four (CFTR and mDRA) experiments. The differences in P_o, NP_o and τ_c exceed $P < 0.01$, whereas the τ_0 values are not different. Time and current scales are given next to the traces. (**i**) Expression levels of CFTR (top) and DRA (middle), and biotinylated CFTR pulled down by avidin (bottom).

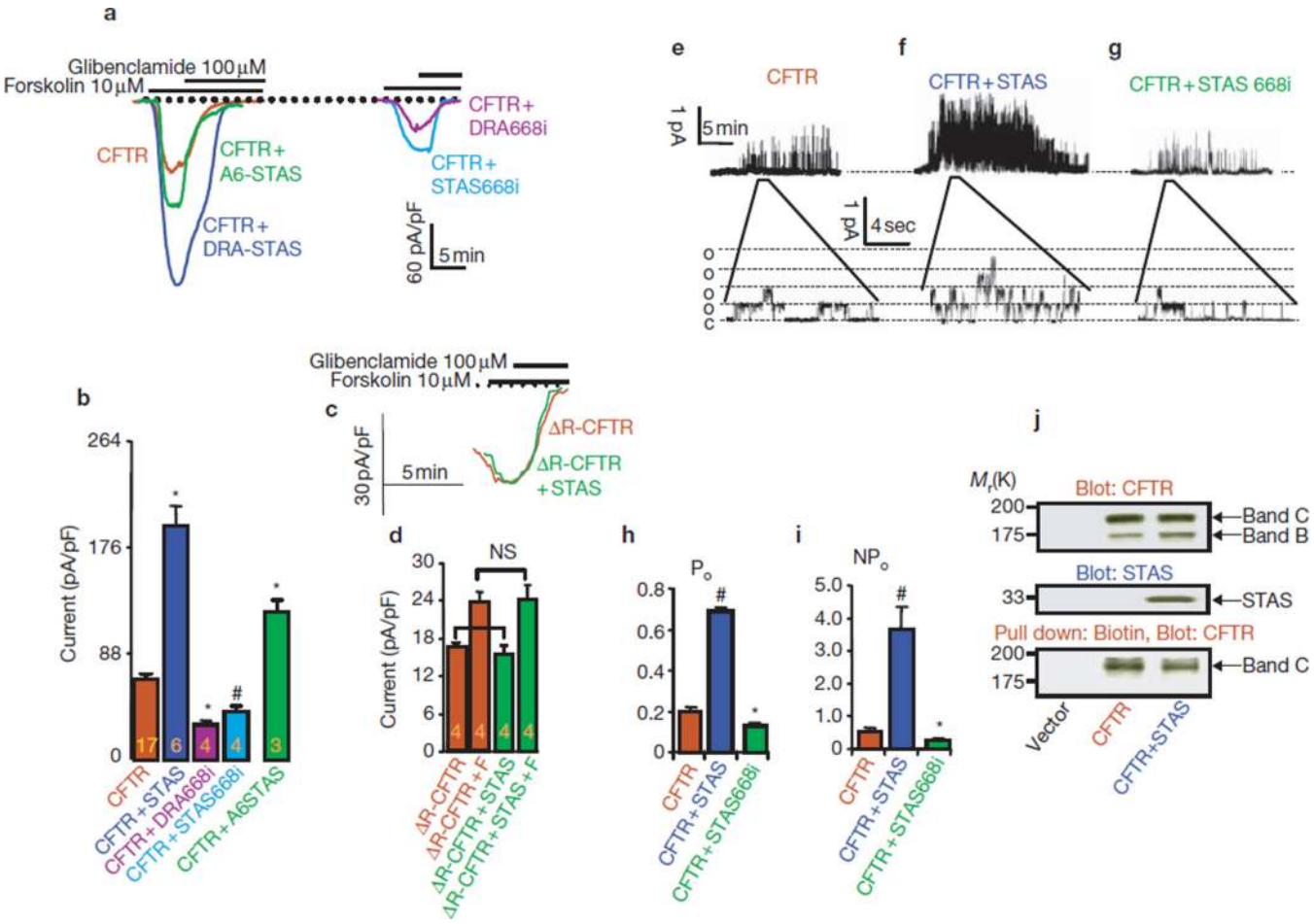

Figure 3.

STAS domain activation of CFTR requires intact STAS and R domains. All traces and averages are colour-coded, as indicated. (**a**) Cells were transfected with CFTR (brown), CFTR and the STAS domain of DRA (blue), CFTR and infused with MBP–STAS domain of mSLC26A6 (green), CFTR and mDRA668i (purple), or CFTR and STAS668i (light blue), and were used to measure forskolin-stimulated whole-cell current. At peak current, the cells were treated with 100 μM glibenclamide. (**b**) Mean ± s.e.m. of the indicated number of experiments. #$P < 0.05$ and *$P < 0.01$, compared with CFTR only. (**c, d**) Cells transfected with ΔR-CFTR (brown), or ΔR-CFTR and STAS domain (green), were used to measure the current before and after stimulation with forskolin (F). NS, not significant. (**e–g**) Single-channel activity was recorded from cells transfected with CFTR (**e**), CFTR and STAS (**f**), or CFTR and STAS668i (**g**). (**h, i**)The recorded P_o (**h**) and NP_o (**i**) are summarized (at least four experiments for each condition); *$P < 0.05$ and #$P < 0.01$, compared with CFTR only. (**j**) Expression levels of CFTR (top) and STAS (middle), and biotinylated CFTR pulled down by avidin (bottom).

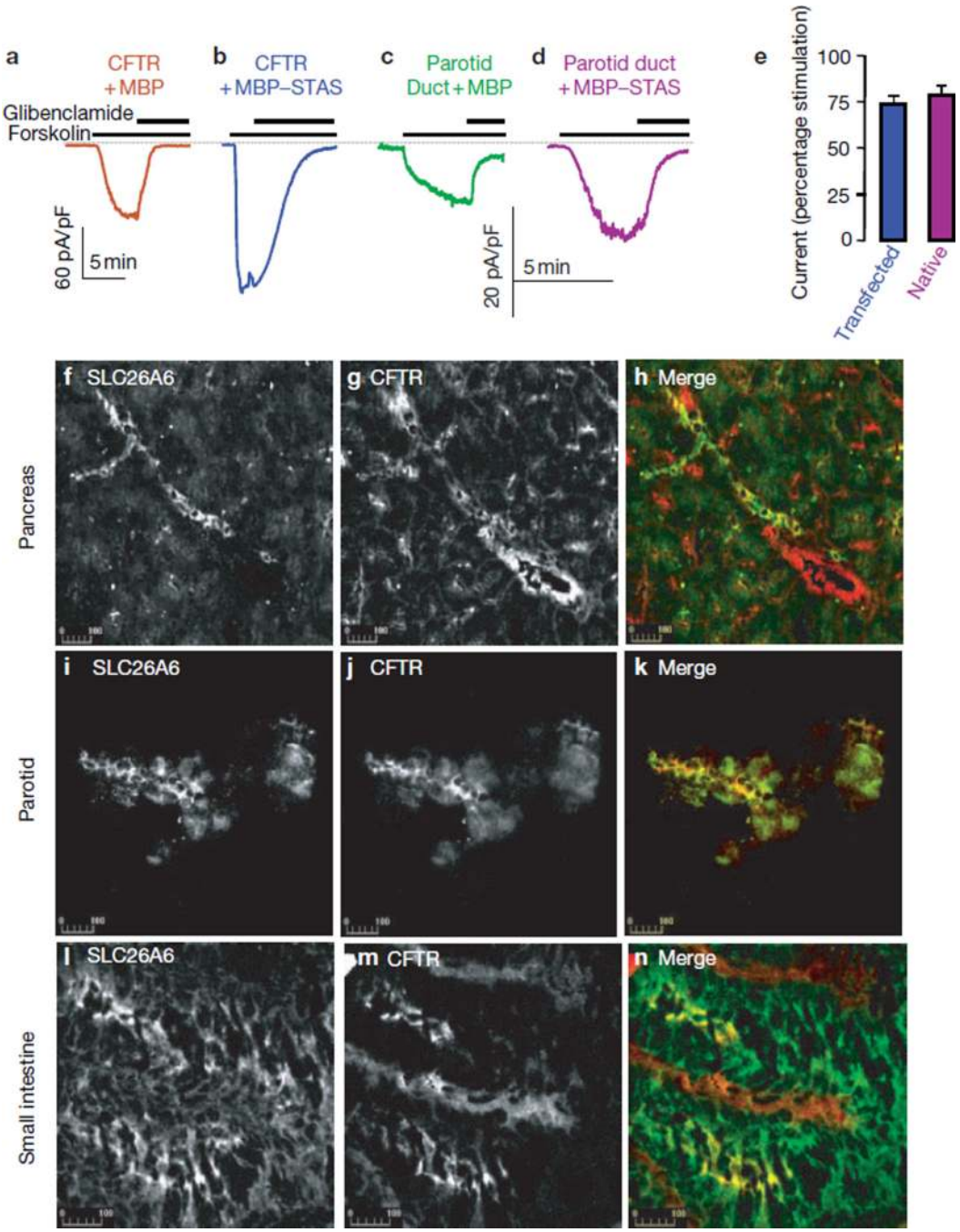

Figure 4.

Activity of STAS *in vivo*. (**a–d**) Activation of native CFTR by the STAS domain. Recombinant MBP (**a, c**) or MBP–STAS (30–100 μg ml^{-1}; **b, d**) were infused into HEK293 cells transfected with CFTR (**a, b**) or duct cells freshly isolated from the parotid gland (**c, d**). After approximately 10 min of infusion, cells were stimulated with forskolin and then inhibited by 100 μM glibenclamide at peak current. (**e**) Summaries of three experiments with transfected CFTR, and five and six experiments with parotid duct cells infused with MBP and MBP-STAS, respectively. The current in **a** was used as the 100% control for **b**. The current in **c** was the 100% control for **d**. All differences from control were statistically

significant ($P < 0.01$). (**f–n**) Co-localization of CFTR and SLC26A6. Sections prepared from the pancreas (**f–h**) and small intestine (**l–n**), and cells prepared from the parotid glands (**i–k**), were fixed and stained with rabbit polyclonal anti-SLC26A6 antibodies (**f, i, l**) and mouse monoclonal anti-CFTR antibodies (**g, j, m**). Merged images are also shown (**h, k** and **n**; SLC26A6 is shown in green, CFTR is shown in red).

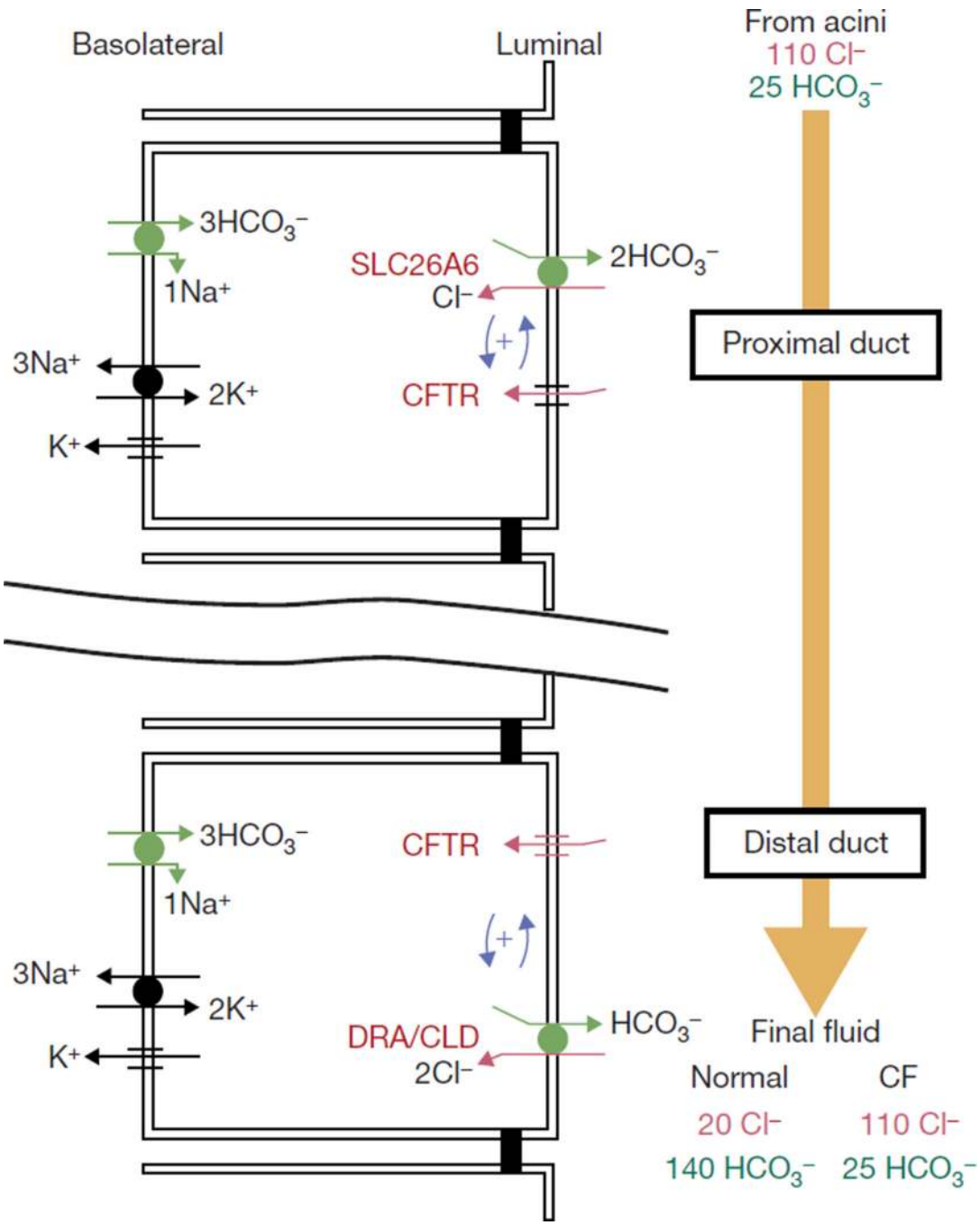

Figure 5.

A model for ductal chloride absorption and bicarbonate secretion. SLC26 transporters and CFTR assemble into a bicarbonate-transporting complex with the aid of their PDZ-binding ligands to facilitate an interaction between the CFTR R-domain and STAS domain of SLC26 transporters. This interaction switches on the activity of both proteins. The consequence of this activation is depicted in the model. Bicarbonate-secreting epithelia express different SLC26 transporters in the proximal and distal portion of the duct, with stoichiometries of two bicarbonates to one chloride and two chlorides to one bicarbonate, together with CFTR. In epithelia, an interaction between CFTR and the SLC26 transporters results in stimulation of CFTR and chloride-bicarbonate exchange[28]. The segment of the

epithelia that expresses a two-bicarbonate/one-chloride transporter absorbs the bulk of the chloride and secretes some bicarbonate, whereas the segment that expresses a two-chloride/one-bicarbonate transporter functions to concentrate the bicarbonate. Disruption of this regulation results in aberrant bicarbonate transport in CF[31], or to CLD and other chloride and bicarbonate transport-related diseases[7].